



INSTITUT DE FRANCE  
Académie des sciences

# *Comptes Rendus*

---

## *Mécanique*

Fatima L. Mota, Luis M. Fabietti, Nathalie Bergeon and Rohit Trivedi

**The effect of confinement on thermal convection and longitudinal macrosegregation in directionally solidified dilute succinonitrile–camphor alloy**


Volume 351, Special Issue S2 (2023), p. 249-262

Published online: 5 January 2023

<https://doi.org/10.5802/crmeca.140>

**Part of Special Issue:** Physical Science in Microgravity within the Thematic Group  
Fundamental and Applied Microgravity

**Guest editors:** Olga Budenkova (CNRS, Université Grenoble Alpes, Grenoble INP, SIMaP, 38000 Grenoble, France), Catherine Colin (IMFT, Université de Toulouse, CNRS, INPT, UPS et GDR 2799 Micropesanteur Fondamentale et Appliquée) and Guillaume Legros (ICARE, CNRS UPR 3021, Univ. Orléans et GDR 2799 Micropesanteur Fondamentale et Appliquée)

 This article is licensed under the  
CREATIVE COMMONS ATTRIBUTION 4.0 INTERNATIONAL LICENSE.  
<http://creativecommons.org/licenses/by/4.0/>



*Les Comptes Rendus. Mécanique sont membres du  
Centre Mersenne pour l'édition scientifique ouverte*

[www.centre-mersenne.org](http://www.centre-mersenne.org)

e-ISSN : 1873-7234



---

Physical Science in Microgravity within the Thematic Group Fundamental and Applied Microgravity / *Sciences physiques en microgravité au sein du GDR Micropesanteur Fondamentale et Appliquée*

# The effect of confinement on thermal convection and longitudinal macrosegregation in directionally solidified dilute succinonitrile–camphor alloy

*L'effet du confinement sur la convection thermique et la macroségrégation longitudinale pendant la solidification dirigée d'un alliage dilué succinonitrile–camphre*

Fatima L. Mota<sup>\*, a, b</sup>, Luis M. Fabietti<sup>b, c, d</sup>, Nathalie Bergeon<sup>a</sup> and Rohit Trivedi<sup>b</sup>

<sup>a</sup> Aix Marseille Univ, Université de Toulon, CNRS, IM2NP, Marseille, France

<sup>b</sup> Iowa State Univ, Dept Mat Sci & Engr, Ames, IA 50010, USA

<sup>c</sup> Universidad Nacional de Córdoba, Facultad de Matemática, Astronomía, Física y Computación, Ciudad Universitaria, 5000 Córdoba, Argentina

<sup>d</sup> Instituto de Física Enrique Gaviola, CONICET, Córdoba, Argentina

*E-mails:* fatima.mota@im2np.fr, fatima.lisboa-mota@im2np.fr (F. L. Mota), fabietti@famaf.unc.edu.ar (L. M. Fabietti), nathalie.bergeon@im2np.fr (N. Bergeon), rohit.trivedi@gmail.com, trivedi@iastate.edu (R. Trivedi)

**Abstract.** Directional solidification experiments were conducted in a succinonitrile–0.24 wt% camphor alloy with an emphasis on the planar front interface temperature dynamics using different sample thicknesses. The interface temperature was found to depend significantly on the thickness due to non-negligible convection effects in the thicker samples. The results were interpreted with the help of an order of magnitude analysis and a boundary layer model, which permitted estimation of the solute macrosegregation profile. The experiments and corresponding analyses performed in this work constitute an experimental characterization of convection effects as a function of sample thickness.

---

\* Corresponding author.

**Résumé.** Des expériences de solidification dirigée ont été menées dans un alliage succinonitrile–0,24% en poids de camphre en se concentrant sur la dynamique de la température de l'interface du front plan en utilisant différentes épaisseurs d'échantillons. La température d'interface s'est avérée dépendre de manière significative de l'épaisseur en raison d'effets de convection non négligeables dans les échantillons plus épais. Les résultats ont été interprétés à l'aide d'une analyse d'ordre de grandeur et d'un modèle de couche limite, qui ont permis d'estimer le profil de macroségrégation du soluté. Les expériences et les analyses correspondantes réalisées dans ce travail constituent une caractérisation expérimentale des effets de convection en fonction de l'épaisseur de l'échantillon.

**Keywords.** Directional solidification, Planar interface dynamics, Convection, Succinonitrile–camphor binary system, Solute boundary layer.

**Mots-clés.** Solidification dirigée, Dynamique des interfaces planes, Convection, Système binaire succinonitrile–camphre, Couche limite solutée.

*Published online: 5 January 2023*

## 1. Introduction

Macroseggregation, i.e. the non-homogeneous macroscopic distribution of alloy components in the solidified casting, can significantly deteriorate the mechanical properties and the processing characteristics of the material. While macroseggregation can usually be kept within acceptable margins, it is desirable to control and minimize it in order to improve and optimize the product quality and process efficiency [1–4]. The metallurgical industry typically faces difficulties in the production of materials free from macroseggregation. Several processes can contribute to the existence of segregation such as long-range diffusion, liquid flow due to shrinkage, melt convection, solid deformation and transport of solid grains/fragments. Natural convection in the melt disturbs the homogeneity of processing conditions in bulk samples and, hence, microstructure formation [5–8]. Two ways are available to get rid of this natural convection in the melt during experiments: under low-gravity conditions or using thin-samples to limit the extent of convection through confinement.

Directional solidification techniques permit study of situations ranging from metal casting to model experiments on interface pattern selection and dynamics [9–11]. It has long been recognized that it is convenient to introduce length scales in the theoretical analysis and modeling of alloy solidification. Two of them can be defined by considering steady-state solidification with planar front: the solutal diffusion length  $l_s$  given by the ratio  $D_L/V$ , with  $D_L$  the solute diffusion coefficient in the melt and  $V$  the pulling velocity; and the thermal diffusion length  $l_T = (k - 1)m_L C_0/kG$ , with  $k$  the solute partition coefficient,  $m_L$  the *liquidus* slope,  $C_0$  the nominal concentration and  $G$  the thermal gradient. The use of thin-sample geometries, where the distance between specimen walls is smaller than, or comparable to, the characteristic microstructure spacing, makes easier the comparison to two-dimensional theories and numerical calculations. This is in part justified by the fact that the solutal diffusion length is typically much larger than the sample thickness [12]. The geometrical confinement imposed in thin-samples is a way to influence the solidification microstructures formation.

Studies on eutectic growth have shown that there is a decisive influence of geometrical constraints on the array geometry, and morphologies in thin specimens vary between the two extreme limits of perfectly circular rods and completely lamellar structures with several distorted rod geometries in between [13, 14]. Confinement can trigger a transition from rods to lamellae, even for growth conditions and alloy compositions where rods would be the preferred morphology in extended systems [15]. The confinement effect on dendritic and cellular microstructures has been extensively studied both experimental and numerically [12, 16–28]. It has already been proven that sample thickness has an influence on cellular branches [29–35] and cell-dendrite transition [36] in directional solidification of binary alloys; the physical reason being that the thickness is shorter than the solutal diffusion length at low velocities [37]. Liu *et al.* [38] and

Athreya *et al.* [16] experimental and numerically studied the effect of dimensionality on microstructures in directional solidified succinonitrile-salol alloys. They were studying the role of confinement in dendritic growth and found that its effects became important when the container size is on the order of the primary dendrite spacing.

In contrast, very little information is available on finite-size effects on the planar front temperature during directional solidification of binary alloys. If local equilibrium conditions at the interface are satisfied and growth is controlled by diffusion, the planar interface temperature at steady-state corresponds to the *solidus* temperature at the nominal alloy concentration  $C_0$ . However, convection in the liquid can be present during growth and makes the steady-state temperature at the front deviate from the *solidus* temperature. For a given thermal gradient  $G$ , there are two critical experimental parameters playing a role on the convection effects: the growth rate and the sample thickness. The convection effects can be made negligible by increasing the growth rate or reducing the sample thickness. Since low velocities are required to maintain a stable planar front during growth, the only choice is to check if the thickness is small enough to make convection effects negligible. The effect of crucible diameter reduction on the convection and macrosegregation has been raised during directional solidification of Pb–Sb alloys [39, 40]. The solutal profiles obtained during plane front solidification are clearly not those expected from a diffusive mass transport. Their segregation pattern indicates extensive convection and mixing during directional solidification. The extent of macrosegregation, however, shows a systematic decrease with the decreasing crucible diameter. So, the intensity of convection decreases while the crucible diameter decreases.

Since the pioneering work of Burton, Prim and Slichter (BPS) [41], simplified models for predicting the longitudinal macrosegregation during crystal growth have been developed by considering the general non-stationary diffusion problem within a zone of extent  $\delta$  in front of the interface, with a melt of spatially uniform composition outside this diffusion layer [42]. Karma *et al.* [43] (KRFT) assumed a non-constant interface velocity, and their model reduces to the previous ones only in the case of both the concentration field and interface velocity being constant. When no convection effects are present in the melt, the purely diffusive limit is found, equivalent to Warren and Langer model [44], which physically corresponds to a boundary layer thickness much larger than the solutal diffusion length  $l_s$ . In the case of convection effects being present, in the limit of an infinite sample length, the melt composition remains constant and equal to the alloy composition, which is equivalent to the well-known segregation equation developed by BPS [41]. In KRFT model, the composition in the solid  $C_s$  is governed by the non-dimensional boundary layer thickness  $\Delta_{\text{KRFT}} = \delta V / D_L$ : the limiting case of diffusive growth occurs when  $\Delta_{\text{KRFT}} \rightarrow \infty$  where  $C_s = C_0$ ; and complete mixing in the liquid occurs when  $\Delta_{\text{KRFT}} \rightarrow 0$  where  $C_s = kC_0$ . The KRFT model is then an improvement of the previous models of macrosegregation, and its basic equations, initially developed for peritectic systems, can be easily adapted to interpret the growth of other binary alloys with a planar solid–liquid interface.

An order of magnitude analysis (OMA) was developed by Camel and Favier [45, 46] for a two-dimensional rectangular solidification system with the growth planar interface parallel to the gravity vector  $g$ . They assumed: negligible convective heat flow (low Prandtl number), adiabatic upper and lower walls, laminar regime (convection not too strong), two-dimensional fluid velocity field and steady fluid motion, a Newtonian fluid and transport properties independent of the temperature and concentration. Their technique consists in non-dimensionalizing the equations of the problem, taking into account the expected variable variations. Then, the non-dimensional coefficients are compared and their order of magnitude evaluated. Different regimes can be defined as a function of the non-dimensional numbers, Grashof–Schmidt  $GrSc = \beta_T g Z^4 / \nu D_L$  and Péclet  $Pe = VZ / D_L$ , where  $\beta_T$  is the thermal expansion coefficient,  $Z$  is the smallest sample dimension between height ( $H$ ) and length ( $L$ ) of the confined liquid zone,  $\nu$  is the kinematic

viscosity, and  $D_L$  is the diffusion coefficient in the liquid. The corresponding limiting lines can be drawn in a diagram that permits analysis of the segregation behavior as a function of the problem's data (Figure 7 of [45] or Figure 4 of [46]). A variety of Péclet number definitions can be found in the literature, the main difference between them lies in the underlying assumptions about solute transport. The authors choose to use the structural definition previously given, where the characteristic length of the system is related to the Bridgman growth configuration.

For a sample of infinite length  $L$  (aspect ratio  $A = L/H$  much higher than 1), two different regimes can be distinguished: a convective–diffusive boundary layer regime where the dominant driving force is the thermal buoyancy driven convection; and a diffusive boundary layer regime where the dominant driving force is the solute rejection at the interface. The convecto-diffusive transition is found when the maximum fluid flow velocity becomes of the order of the diffusion rate imposed by solidification (i.e. the growth rate) [47]. The transition is given by:

$$Gr Sc = Pe^4 \quad \text{if } \{Pe > 5 \text{ and } Gr Sc > 625\} \quad (1)$$

$$Gr Sc = 125Pe \quad \text{if } \left\{ \frac{1}{A} < Pe \text{ and } \frac{125}{A} < Gr Sc < 625 \right\}. \quad (2)$$

For a sample of finite length, there is an additional limited diffusion regime where solute diffusion extends over the whole liquid length ( $Pe < 1/A$  and  $Gr Sc < 125/A$ ). Looking at (1) and the definitions of  $Pe$  and  $Gr Sc$ , for a given thermal gradient  $G$  on Earth ( $g = 9.81 \text{ m/s}^2$ ), the convecto-diffusive transition depends only on the pulling rate  $V$ . However, in the region defined by (2), dependence is seen on the pulling rate  $V$  and the smallest dimension of the sample.

There is a good qualitative agreement between this analysis and experimental results obtained during solidification of metallic alloys and semiconductors (Figure 4 of [46]). In order to get rid of convection effects, one can rather increase the pulling rate or decrease the sample thickness. Based on the previous equations, for a given pulling rate  $V$  and thermal gradient  $G$ , the critical dimension limiting the transition between convective–diffusive boundary layer and diffusive boundary layer regimes can be estimated using the relation:

$$H_c = \left( \frac{125V\nu}{\beta_T g G} \right)^{\frac{1}{3}}. \quad (3)$$

The OMA described above was developed for the solidification of a doped metal or semiconductor in a simplified horizontal Bridgman crystal growth configuration. These kind of materials have a low Prandtl number ( $Pr$ ), which means that the thermal diffusion is very quick in comparison to the momentum transport diffusion. However, as evidenced in their work, there is a wide range of control parameters where solute convective transport occurs, while heat transfer remains mainly conductive. For example, for an aluminum (Al)–0.4 wt% copper (Cu) alloy, whose thermal diffusion length is one order of magnitude higher than the solutal diffusion length, one may have a solutal diffusion-controlled growth if the experiments are performed in reduced gravity. The comparison between the obtained laws of the OMA and experimental literature results did not concern any organic material that, in general, presented Prandtl numbers higher than 1. In the present work, the validity of this OMA will be tested for the organic transparent alloy succinonitrile (SCN)–camphor ( $Pr \approx 20$ ). This transparent organic analog behaves like metallic alloys concerning solidification and its main advantages are: transparency to visible light, so that *in situ* and real time observation of the interface can be made by classical optical techniques; and low melting temperature ( $\approx 58 \text{ }^\circ\text{C}$ ), which simplifies the design of the Bridgman furnace. Based on the material properties (Table 1) and the imposed experimental conditions (described in later sections), one would have solidification controlled by solutal diffusion. But it will be shown that there is a range of parameters for which it is not the case. In that way, thin-sample directional solidification experiments with stable planar front growth were realized with different sample thicknesses.

The experimental data were further interpreted using a boundary layer model of planar interface dynamics allowing to access quantitatively the effect of convection [43].

## 2. Experimental procedure

The SCN was purified by distillation under vacuum followed by zone refining as in previous works [48]. The purity was characterized by the freezing range (0.003 °C) which corresponds to 99.9998%. Camphor was sublimated under vacuum from the 98% commercial product. An alloy of 0.24 wt% camphor composition was prepared inside the glovebox under the protection of high-purity nitrogen. Nitrogen atmosphere was preferred over argon because previous studies have shown that the addition of argon provides a dilute solute with SCN [49, 50].

For the directional solidification experiments, the liquid alloy was introduced into rectangular thin sandwiched glass cells (4 × 300 mm) of different thicknesses (from 12.5 to 200 μm) inside the glovebox under high-purity nitrogen atmosphere. Two additional cells, identical to the sample cells, were also prepared with pure SCN and eutectic composition (23.6 wt% camphor). These additional cells were placed on the two sides of the sample cell, and the three-cell assembly was placed in the temperature gradient stage for stabilization. The hot and cold baths were maintained at 97 and 3.5 °C, respectively, yielding a nominal thermal gradient of 78 °C/cm based on the pure SCN and eutectic positions and their respective known temperatures (58.08 and 37.7 °C [51]). The gradient measurement was double checked using a sample similar to those used in directional solidification experiments but filled with a K-type thermocouple and pure SCN. The gradient was measured by pushing the thermocouple into the hot zone one centimeter and pulling it out at a velocity of 2.5 μm/s. This allowed the measured position of the thermocouple to be related to the sampled temperature by time. The measured gradient, 74 °C/cm, was the result of a linear fit of the temperature–distance relationship. The samples were then directionally solidified at a constant pulling velocity  $V$  for a long time until the presence of steady-state growth was established. The evolution of interface position with time was measured and the interface temperature was determined from its position knowing the pure SCN position and the thermal gradient.

## 3. Results and discussion

The binary alloy, SCN–0.24 wt% camphor, was solidified by pulling through a fixed thermal gradient. The planar solid–liquid interface can be destabilized by increasing the velocity, thus giving rise to cellular or dendritic microstructures. The critical velocity  $V_c$  leading to the transition from a planar to a cellular front can be calculated using the Mullins–Sekerka linear stability analysis [52],  $V_c = kGD_L/(k-1)m_L C_0$ , and is equal to 0.48 μm/s (material properties given in Table 1). Although, the main focus of this work was on planar front temperature ( $V$  should be lower than  $V_c$ ), some directional solidification experiments were performed with a pulling rate higher than  $V_c$  ( $V = 1$  μm/s) using samples of thicknesses between 25 and 100 μm. Under these experimental conditions, the morphological instability appeared at the interface after the initial transient, and cellular patterns were obtained in steady-state growth (Figure 1). For  $V = 1$  μm/s, the solutal diffusion length (270 μm) is higher than the sample thickness leading to effects on cellular branches. As previously reported in the literature [16, 35, 38], the confinement has an effect on the primary spacing  $\lambda$ , defined as the distance between the cell center and its closest neighbors. The characteristic microstructure spacing, which is higher or comparable to the distance between specimen walls, decreases with the increase of thickness. In order to keep a stable planar front till steady-state growth, a pulling rate of 0.3 μm/s ( $\ll V_c$ ) was chosen in the following experiments.

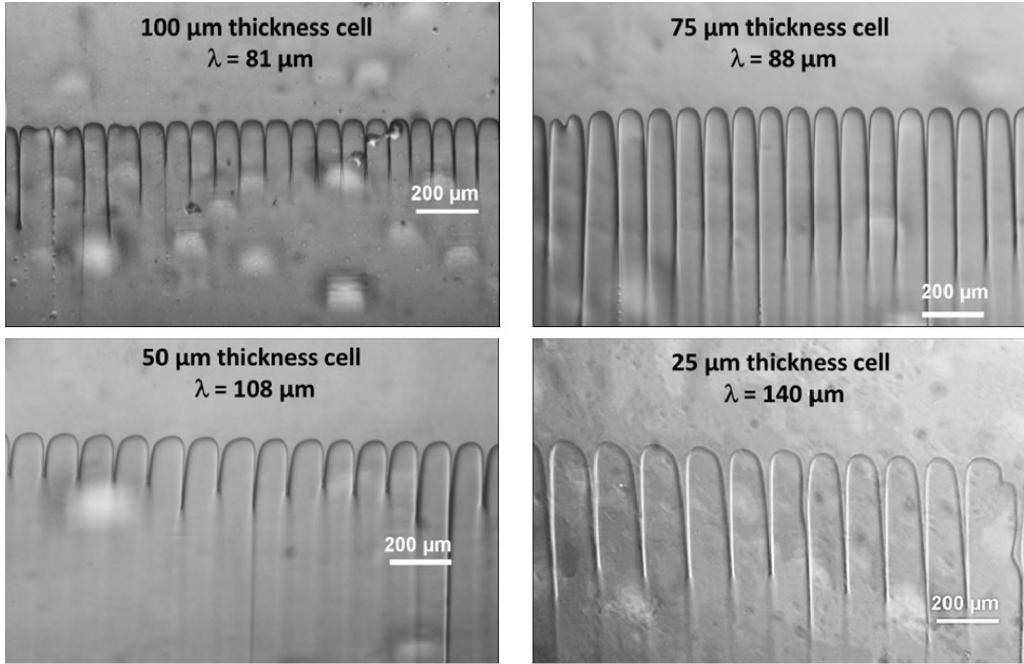


**Figure 1.** Steady-state growth morphology of SCN-0.24 wt% camphor alloy directionally solidified at  $V = 1 \mu\text{m/s}$  and  $G = 78 \text{ }^\circ\text{C/cm}$  in samples of different thicknesses. The sample thickness and the primary spacing ( $\lambda$ ) are given in each picture.

**Table 1.** Properties of succinonitrile and succinonitrile-0.24 wt% camphor alloy.

Thermal expansion coefficient ( $\beta_T$ ) [53]	$7.85 \times 10^{-4} \text{ K}^{-1}$
Solutal expansion coefficient ( $\beta_c$ ) [54]	$1.73 \times 10^{-4} \text{ wt}\%^{-1}$
Kinetic viscosity ( $\nu$ ) [55]	$2.6 \text{ mm}^2/\text{s}$
<i>Liquidus</i> slope ( $m_L$ ) [56]	$-1.365 \text{ K/wt}\%$
<i>Liquidus</i> temperature ( $T_L$ ) [56]	$57.7 \text{ }^\circ\text{C}$
<i>Solidus</i> temperature ( $T_s$ ) [51]	$53.5 \text{ }^\circ\text{C}$
Solute partition coefficient ( $k$ ) [51]	0.07
Solute diffusion coefficient in the liquid ( $D_L$ ) [56]	$270 \mu\text{m}^2/\text{s}$
Thermal diffusion coefficient ( $D_{th}$ ) [56]	$1.15 \times 10^5 \mu\text{m}^2/\text{s}$

The sample thicknesses were selected based on the universal diagram developed by Camel and Favier [45,46], reproduced in Figure 2 for the Péclet ( $Pe$ ) and Grashof-Schmidt ( $GrSc$ ) ranges used in this work. In the definition of the  $Pe$  number used by these authors,  $Z$  is the smaller of the dimensions between the height and length of the confined liquid region. In thin-samples, the thickness (or height) is much lower than the length, and is then used as the characteristic dimension of the system to estimate  $Pe$  number. For the experimentally applied thermal gradient  $G = 78 \text{ }^\circ\text{C/cm}$ , several red dashed lines were drawn in Figure 2, which represent constant pulling rate with increasing sample thickness  $H$  along the line. Applying (3) with  $V = 0.3 \mu\text{m/s}$ , a critical dimension of  $117 \mu\text{m}$  was found, corresponding to the transition between convecto-diffusive and diffusive regimes. Given this critical value, different sample thicknesses ( $H$ ) were selected

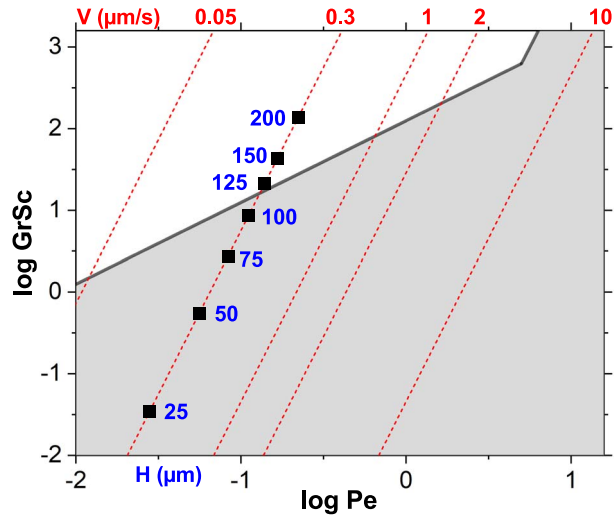


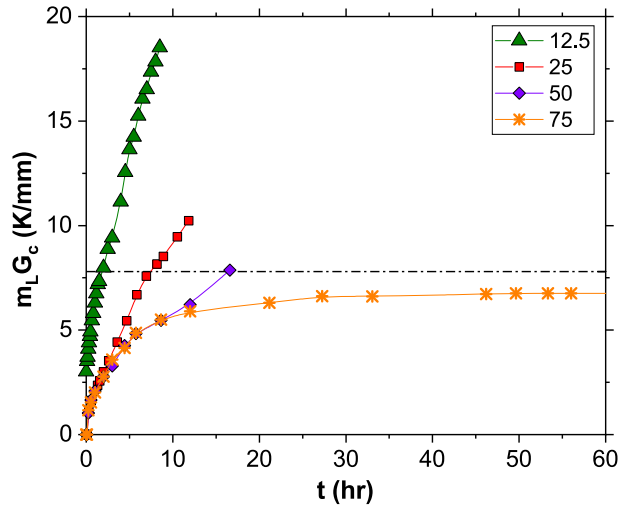
**Figure 2.** Grashof–Schmidt versus Péclet number diagram [45, 46], where the white region corresponds to convective–diffusive boundary layer regime and the grey shaded region correspond to diffusive boundary layer regime. The red dashed lines represent constant pulling velocity  $V$ . The square markers represent different sample thickness  $H$ .

to perform directional solidification experiments, evidenced by the different markers over the  $V = 0.3 \mu\text{m/s}$  line in Figure 2.

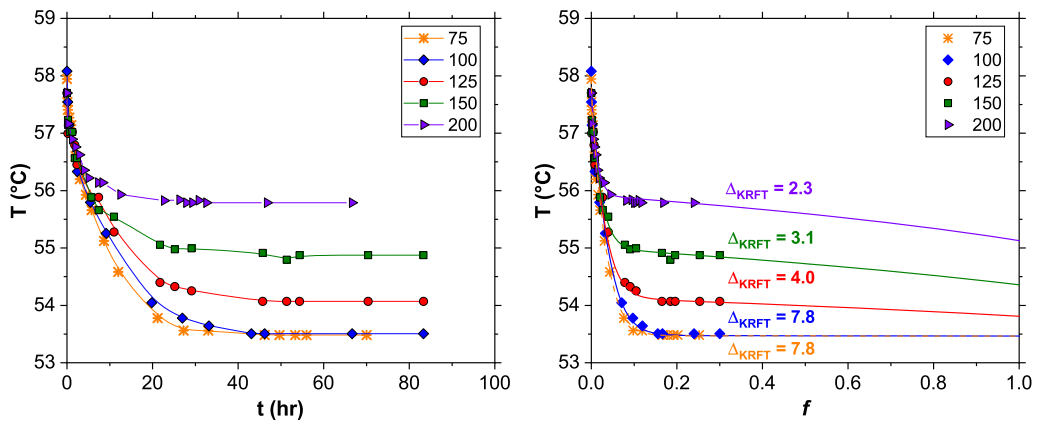
For some of the samples directionally solidified at  $V = 0.3 \mu\text{m/s}$ , the interface broke up before reaching a steady state with a temperature below the theoretical *solidus* temperature. This happened in the samples with thicknesses 12.5, 25 and  $50 \mu\text{m}$ . The most likely reason was the presence of a meniscus, which deformed the interface and shifted the threshold of critical velocity to a lower value [57, 58]. Furthermore, a linear relationship between the break time and the sample thickness was observed. The interface position data as function of time were manipulated in order to obtain the interface velocity and the solid composition at the interface. The constitutional supercooling criterion [59, 60] assumes that any perturbation at the flat interface will grow if  $G - m_L G_c < 0$ , where  $G_c$  is the concentration gradient in the liquid at the interface. This criterion was fulfilled for thicknesses lower than  $75 \mu\text{m}$ , as evidenced by the evolution of the concentration gradient in the liquid at the interface (Figure 3). These results are in agreement with the previous findings of De Cheveigné *et al.* [57]. They found that the meniscus affects a distance of about  $50 \mu\text{m}$ , which is of the order of the sample thickness range over which the threshold pulling rate is seen to vary.

Figure 4(a) shows the evolution of the planar front interface temperature for samples of different thicknesses (higher than  $50 \mu\text{m}$ ), directionally solidified at  $V = 0.3 \mu\text{m/s}$  and  $G = 78 \text{ }^\circ\text{C/cm}$ . There was a non-negligible effect of the thickness on steady-state temperature. The criterion applied to stop the experiments was that the difference between the interface temperature was not visible for a period of time higher than 30 h. The thermal diffusivity in organic alloys is several orders of magnitude higher than the solute diffusivity ( $D_{\text{th}}$  and  $D_L$ , respectively, in Table 1), which means that heat diffusion is much faster than solute diffusion. Thus, slow solute diffusion is often the limiting physical process and the solute diffusion length  $l_s = D_L/V$  is the most important scale (or in the time scale,  $t_s = D_L/V^2$ ). For the SCN–0.24 wt% camphor alloy solidified at  $V = 0.3 \mu\text{m/s}$ ,  $l_s = 900 \mu\text{m}$  and  $t_s = 0.83 \text{ h}$ , which means that 30 h of *plateau* are more than 30 times longer than this limiting time scale. The planar front temperature found for the sample





**Figure 3.** Concentration gradient in the liquid at the interface,  $m_L G_c$ , as function of time  $t$  for the SCN-0.24 wt% camphor alloy solidified at  $V = 0.3 \mu\text{m/s}$  and  $G = 78 \text{ }^\circ\text{C/cm}$  in thin-samples of different thicknesses.



**Figure 4.** Planar interface temperature  $T$  as function of (a) time  $t$  and (b) solidified fraction  $f$ , for a SCN-0.24 wt% camphor alloy directionally solidified at  $V = 0.3 \mu\text{m/s}$  and  $G = 78 \text{ }^\circ\text{C/cm}$  in samples of different thicknesses. The curves in (b) correspond to the calculated profiles using KRFT model [43] with different  $\Delta$  values.

of thickness  $100 \mu\text{m}$  ( $53.5 \text{ }^\circ\text{C}$ ) is in good agreement with the previously reported *solidus* temperature  $T_s$  [51]. Teng and Liu [56] measured the steady-state planar interface temperature during directional solidification of a SCN-0.35 wt% camphor alloy on  $200 \mu\text{m}$  thick samples, and found a steady-state temperature of  $55.7 \text{ }^\circ\text{C}$ . The result obtained in this work for a sample of thickness  $200 \mu\text{m}$  ( $55.8 \text{ }^\circ\text{C}$ ) also highlights the reproducibility of the results: a slightly higher temperature was measured for a slightly lower concentration, as theoretically predicted by the phase diagram [51].

These results can be further interpreted using a boundary layer model of transient planar interface dynamics. Considering the growth of only one solid phase, the basic equations of the KRFT model [43] were used to fit the experimental data of the planar interface temperature

**Table 2.** Non-dimensional boundary layer thickness using KRFT model [43] and OMA analysis [45,46,61], and relative importance of solutally driven flow [62] defined by the ratio  $V_c/V_T$ .

Sample thickness ( $\mu\text{m}$ )	$\Delta_{\text{KRFT}}$	$\Delta$	$\Delta_{\text{KRFT},c}$	$V_c/V_T$
75	7.8	1.00	1.00	14.4
100	7.8	1.00	1.00	8.1
125	4.0	0.83	0.98	3.6
150	3.1	0.48	0.95	0.8
200	2.3	0.20	0.90	0.1

(Figure 4(b)). The calculations were realized assuming a sample length of 725 mm in the model, but the solidified fraction  $f$  in Figure 4(b) was calculated as the ratio between the solidified length  $Vt$  and the experimental sample length  $L = 300$  mm. All these experiments were performed with the same control parameters ( $C_0$ ,  $G$  and  $V$ ), the only difference being the sample thickness. Considering an infinite sample length ( $L \gg l_s = 900 \mu\text{m}$ ), different  $\Delta_{\text{KRFT}}$  values were used to fit the experimental data which increased with decreasing sample thickness (Table 2). This means that the boundary layer decreases with sample thickness, and becomes of the same order as the diffusion layer for the highest thickness. It should be mentioned that the curves for the 100 and 75  $\mu\text{m}$  thickness samples were labeled with  $\Delta_{\text{KRFT}} = 7.8$ , but any value of  $\Delta$  higher than 7.8 leads to similar results, which in turn correspond to those of the Warren and Larger model [44]. This means that this value of  $\Delta_{\text{KRFT}}$  is slightly higher than the threshold at which convection effects become negligible.

As previously mentioned, the experiments were stopped after about 100 h of solidification because the interface was not moving, at least for the last 30 h, so steady-state was considered to have been reached. However, the model curves show that this was the case only for the 100 and 75  $\mu\text{m}$  thickness samples (Figure 4(b)). In all the other experiments, the interface was still moving but at a very slow drifting rate ( $<0.15$   $^{\circ}\text{C}/\text{day}$ ), that it was very difficult to see, if not impossible, within the experimental error. For example, based on the KRFT model results, the planar interface temperature of the 125  $\mu\text{m}$  thick sample would take at least another 47 days to reach the *solidus* temperature. It would be exceedingly difficult to perform a solidification experiment during such a long period of time. One of the advantages of the model is that it allows the experimental data to be extrapolated and, consequently, the results to be better interpreted.

The segregation profiles could be calculated using the KRFT model [43] (Figure 5). In the limiting case of diffusive growth (dashed line), the solute distribution can be divided into three regions, i.e. initial transient, steady state growth and the final transient region. The complete mixing in the liquid is traduced by a convex profile (dotted line). For intermediate values of  $\Delta_{\text{KRFT}}$ , the S-shaped segregation profiles are very different from the two boundary profiles. The calculated profiles soon deviate from the diffusion profile, thus illustrating the blocking of the pure diffusion profile over a finite distance ahead of the interface. However, even for the highest sample thickness, 200  $\mu\text{m}$ , the complete mixing is still a long way off. Sample thickness does indeed have a non-negligible effect on the longitudinal macrosegregation.

In their order and magnitude analysis, Camel and Favier [45, 46] also included a solute boundary layer  $\delta$  (or  $\Delta = \delta V/D_L$ ), which can be determined as function of the problem data. With this parameter, boundary layer models can be used to discuss longitudinal segregation: in a diffusive regime  $\Delta = 1$ ; in a convective-diffusive regime  $\Delta = 125(Pe/GrSc)$  (Figure 5 of [46]). The  $\Delta$  values were estimated based on Figure 2 for the studied thicknesses (Table 2), and they are quite different from those used in the KRFT model (Figure 4b and  $\Delta_{\text{KRFT}}$  in Table 2). However, as discussed in detail by Camel and Favier [61], the  $\Delta_{\text{KRFT}}$  values should not be compared directly

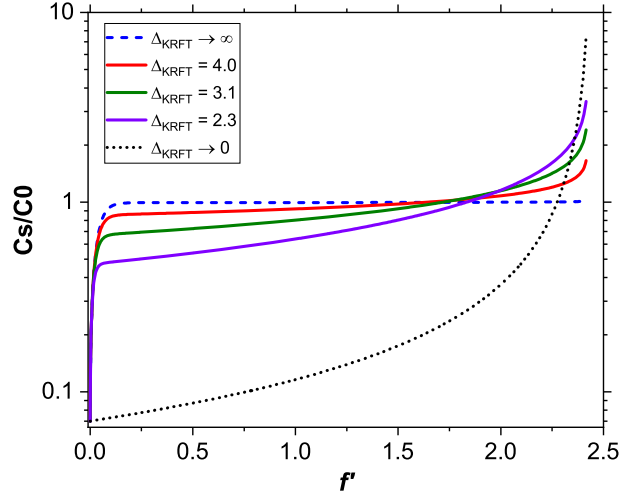


**Figure 5.** Segregation profiles calculated using KRFT model [43] with different  $\Delta_{\text{KRFT}}$  values as function of the solidified fraction  $f'$ .  $f'$  is the ratio of the solidified length to the sample length used in the model. SCN–0.24 wt% camphor alloy,  $V = 0.3 \mu\text{m/s}$  and  $G = 78 \text{ }^\circ\text{C/cm}$ .

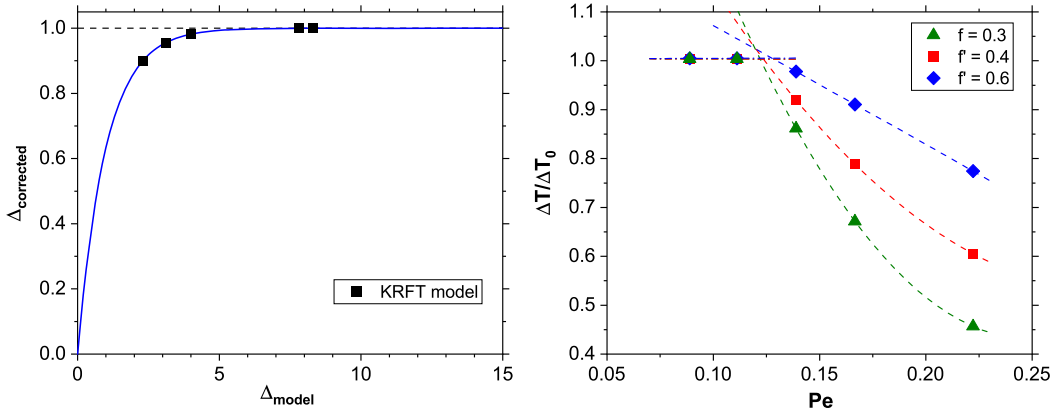


**Figure 6.** (a) Correction of the non-dimensional boundary layer thickness used in models like KRFT [43]. (b) Dimensionless undercooling ( $\Delta T/\Delta T_0$ ) as a function of Péclet number ( $Pe$ ) for different solidified fractions  $f$ .

with those arising from the boundary layer  $\Delta$ , but they should be corrected  $\Delta_{\text{KRFT},c} = 1 - e^{-\Delta_{\text{KRFT}}}$  (Figure 6(a)). Even if there is still a difference between the corrected values  $\Delta_{\text{KRFT},c}$  and the boundary layer  $\Delta$  (Table 2), both results underline that there is a sample thickness between 100 and 125  $\mu\text{m}$  corresponding to the dominant transport mode transition.

A weakness of the OMA developed by Camel and Favier [45, 46] is that the relative importance of solutally driven flow is not estimated. Garandet and Alboussiere [62] proposed to estimate this relative importance, at the scale of the boundary layer thickness, using the ratio of the solute-driven  $[V_c(\delta)]$  and thermally  $[V_T(\delta)]$  driven natural convection flow velocities:

$$\frac{V_c(\delta)}{V_T(\delta)} = \frac{\beta_c G_c}{\beta_T G} \left( \frac{\Delta}{Pe} \right)^2 \quad (4)$$

with  $\beta_c$  the solutal expansion coefficient and  $G_c$  the composition gradient at the interface ( $G_c = VC_0(1-k)/D_Lk$ ). The solute driven fluid flow was at most, of the same order for the smaller thicknesses, meaning that solutal convection dominated thermal convection, in contrast to the highest thicknesses (Table 2). For 125  $\mu\text{m}$ , the solutal convection appeared to be dominant, but the effects of thermal convection cannot be neglected, as evidenced by the previous analyses.

The effect of thickness can also be analyzed by representing dimensionless undercooling as function of Péclet number (Figure 6(b)). The dimensionless undercooling was estimated using the relation:

$$\frac{\Delta T}{\Delta T_0} = \frac{T_L - T}{T_L - T_S} \quad (5)$$

where  $T_L$  and  $T_S$  are the *liquidus* and *solidus* temperatures for SCN–0.24 wt% camphor, respectively 57.7 and 53.5  $^{\circ}\text{C}$ , and  $T$  is the interface temperature. The green triangles in Figure 6(b) correspond to the experimental data; experiments were stopped after 100 h of solidification which corresponds to a solidified fraction of  $f \approx 0.3$ . The red squares and blue diamonds correspond to  $f'$  equal to 0.4 and 0.6, respectively, and could be represented using the boundary layer model results. For solidified fractions higher than 0.6, the segregation profiles have a strong effect of the sample end and the final transient, leading to a rapid decrease in the interface temperature (Figure 5). This was the reason why solidified fractions higher than 0.6 were not compared with the experimental results. Two different regions can be distinguished: one where the dimensionless undercooling is constant and does not depend on  $f$ ; and another where the dimensionless undercooling depends on  $Pe$  and also on  $f$ . The existence of these two different regimes is an evidence of the change in the dominant transport mode. Tendency curves were plotted for each data-set and for each of the regions. For each data-set, the tendency curves of the two regions intersect at  $Pe \approx 0.12$ , corresponding to a thickness  $H \approx 112 \mu\text{m}$ . This value is very close to the estimated using the order and magnitude analysis of Camel and Favier [45, 46] ( $H_c = 117 \mu\text{m}$ ).

#### 4. Conclusion

The effect of sample thickness on interface stability and cell/dendrite shape during directional solidification had already been examined in the literature. However, the effect of thickness on the interface temperature during steady-state planar front growth had not been studied. In this work, directional solidification experiments were performed on a succinonitrile–0.24 wt% camphor alloy using sample thicknesses between 75 and 200  $\mu\text{m}$ . The imposed experimental conditions, pulling rate  $V = 0.3 \mu\text{m/s}$  and thermal gradient  $G = 78 \text{ }^{\circ}\text{C/cm}$ , were set in order to keep a planar front throughout the experiment. The temperature of the planar front was found to depend on the sample thickness. The experiments were stopped after 100 h of solidification because the interface temperature was not changing in several consecutive measurements, so steady-state growth was considered to have been reached. The experimental results were analyzed using a boundary layer model of transient planar interface dynamics. In some experiments, in particular, those with sample thickness higher than 125  $\mu\text{m}$ , the interface was still moving when they were stopped, but at such a slow rate that it was not possible to notice it visually. An order and magnitude analysis allowed to realize that for a given growth velocity and thermal gradient, there is a critical Péclet number (equivalent to thickness) above which convection effects became non-negligible. This critical thickness was estimated to be 117  $\mu\text{m}$ , which is in good agreement with that estimated based on the experimental and boundary layer model results (112  $\mu\text{m}$ ). The experimental results and the respective analyses showed that above a given thickness, another mechanism besides diffusion was activated, that contributed to the solute removal in front of the interface. This mechanism is associated with convection of thermal origin. The results found in this work provide experimental proof of the effect of thickness on macrosegregation profiles during planar front directional solidification.

## Conflicts of interest

The authors declare no competing financial interest.

## Dedication

The manuscript was written through contributions of all authors. All authors have given approval to the final version of the manuscript.

## Acknowledgments

The authors gratefully acknowledge fruitful discussions with B. Billia. The authors express their gratitude to CNES and NASA (through Grant no. NNX12AK54G) for the support received in the scientific projects MISOL3D (Microstructures de SOLidification 3D) and DSIP (Dynamical Selection of Interface Patterns).

## References

- [1] J. Li, M. H. Wu, A. Ludwig, A. Kharicha, "Simulation of macrosegregation in a 2.45-ton steel ingot using a three-phase mixed columnar-equiaxed model", *Int. J. Heat Mass Transfer* **72** (2014), p. 668-679.
- [2] E. J. Pickering, C. Chesman, S. Al-Bermani, M. Holland, P. Davies, J. Talamantes-Silva, "A comprehensive case study of macrosegregation in a steel ingot", *Metall. Mater. Trans. B* **46** (2015), p. 1860-1874.
- [3] K. V. S. Rao, "Experimental studies on microstructure evolution and macro segregation during upward directional solidification of lead-tin alloys", *Proc. Mater. Sci.* **5** (2014), p. 1224-1230.
- [4] M. Chatelain, M. Albaric, D. Pelletier, V. Botton, "Solute segregation in directional solidification: Scaling analysis of the solute boundary layer coupled with transient hydrodynamic simulations", *J. Cryst. Growth* **430** (2015), p. 138-147.
- [5] M. E. Glicksman, S. R. Coriell, G. B. Mcfadden, "Interaction of flows with the crystal-melt interface", *Annu. Rev. Fluid Mech.* **18** (1986), p. 307-335.
- [6] S. H. Davis, "Hydrodynamic interactions in directional solidification", *J. Fluid Mech.* **212** (1990), p. 241-262.
- [7] M. D. Dupouy, D. Camel, J. J. Favier, "Natural-convection in directional dendritic solidification of metallic alloys. I. Macroscopic effects", *Acta Metall.* **37** (1989), p. 1143-1157.
- [8] H. Nguyen-Thi, G. Reinhart, B. Billia, "On the interest of microgravity experimentation for studying convective effects during the directional solidification of metal alloys", *C. R. Méc.* **345** (2017), p. 66-77.
- [9] W. Kurz, D. J. Fisher, *Fundamentals of Solidification*, Trans Tech Publications, New Hampshire, USA, 1998.
- [10] M. Cross, H. Greenside, *Pattern Formation and Dynamics in Nonequilibrium Systems*, Cambridge University Press, Cambridge, 2009.
- [11] J. A. Dantzig, M. Rappaz, *Solidification*, EPFL Press, Lausanne, 2009.
- [12] S. Gurevich, A. Karma, M. Plapp, R. Trivedi, "Phase-field study of three-dimensional steady-state growth shapes in directional solidification", *Phys. Rev. E* **81** (2010), article no. 011603.
- [13] M. Serefoglu, R. E. Napolitano, "On the selection of rod-type eutectic morphologies: Geometrical constraint and array orientation", *Acta Mater.* **56** (2008), p. 3862-3873.
- [14] V. T. Witusiewicz, U. Hecht, S. Rex, "Fibrous eutectic growth in succinonitrile-neopentylglycol-(D)camphor-aminomethylpropanediol alloys for thin and bulk sample geometry", *Acta Mater.* **65** (2014), p. 360-372.
- [15] M. Serefoglu, R. E. Napolitano, M. Plapp, "Phase-field investigation of rod eutectic morphologies under geometrical confinement", *Phys. Rev. E* **84** (2011), article no. 011614.
- [16] B. P. Athreya, J. A. Dantzig, S. Liu, R. Trivedi, "On the role of confinement on solidification in pure materials and binary alloys", *Philos. Mag.* **86** (2006), p. 3739-3756.
- [17] N. F. Dean, A. Mortensen, M. C. Flemings, "Steady-state cellular solidification of Al-Cu reinforced with alumina fibers", *Metall. Mater. Trans. A* **26** (1995), p. 2141-2153.
- [18] L. M. Fabietti, J. A. Sekhar, "Planar to equiaxed transition in the presence of an external wetting surface", *Metall. Mater. Trans. A* **23** (1992), p. 3361-3368.
- [19] L. M. Fabietti, J. A. Sekhar, "Quantitative microstructure maps for restrained directional growth", *J. Mater. Sci.* **29** (1994), p. 473-477.
- [20] J. D. Hunt, S. Z. Lu, "Numerical modeling of cellular and dendritic array growth – spacing and structure predictions", *Mater. Sci. Eng. A* **173** (1993), p. 79-83.

- [21] J. H. Jeong, N. Goldenfeld, J. A. Dantzig, "Phase field model for three-dimensional dendritic growth with fluid flow", *Phys. Rev. E* **64** (2001), article no. 041602.
- [22] L. X. Liu, J. S. Kirkaldy, "Systematics of thin-film cellular dendrites and the cell-to-dendrite transition in succinonitrile salol, succinonitrile acetone and pivalic acid ethanol", *J. Cryst. Growth* **140** (1994), p. 115-122.
- [23] S. Z. Lu, J. D. Hunt, "A numerical-analysis of dendritic and cellular array growth – the spacing adjustment mechanisms", *J. Cryst. Growth* **123** (1992), p. 17-34.
- [24] M. Plapp, M. Dejmek, "Stability of hexagonal solidification patterns", *Europhys. Lett.* **65** (2004), p. 276-282.
- [25] J. A. Sekhar, R. Trivedi, "Development of solidification microstructures in the presence of fibers or channels of finite width", *Mater. Sci. Eng. A* **114** (1989), p. 133-146.
- [26] A. Semoroz, S. Henry, M. Rappaz, "Application of the phase-field method to the solidification of hot-dipped galvanized coatings", *Metall. Mater. Trans. A* **31** (2000), p. 487-495.
- [27] D. Shanguan, J. D. Hunt, "In situ observation of nonfaceted cellular growth in a narrow channel", *Metall. Trans. A* **22** (1991), p. 1683-1687.
- [28] R. Trivedi, H. Miyahara, P. Mazumder, E. Simsek, S. N. Tewari, "Directional solidification microstructures in diffusive and convective regimes", *J. Cryst. Growth* **222** (2001), p. 365-379.
- [29] M. A. Eshelman, V. Seetharaman, R. Trivedi, "Cellular spacings—I. Steady-state growth", *Acta Metall.* **36** (1988), p. 1165-1174.
- [30] S. H. Han, R. Trivedi, "Primary spacing selection in directionally solidified alloys", *Acta Metall. Mater.* **42** (1994), p. 25-41.
- [31] J. S. Kirkaldy, "Spontaneous evolution of microstructure in materials", *Metall. Trans. A* **24** (1993), p. 1689-1721.
- [32] L. X. Liu, J. S. Kirkaldy, "Relationship between free and forced velocity or cellular dendrites", *Scr. Metall. Mater.* **29** (1993), p. 801-806.
- [33] L. X. Liu, J. S. Kirkaldy, "Systematics of pattern parameters in steady-state solidification of succinonitrile-salol, succinonitrile-acetone and pivalic acid-ethanol", *Scr. Metall. Mater.* **28** (1993), p. 1029-1034.
- [34] L. X. Liu, J. S. Kirkaldy, "Thin-film forced velocity cells and cellular dendrites. 1. Experiments", *Acta Metall. Mater.* **43** (1995), p. 2891-2904.
- [35] K. Somboonsuk, J. T. Mason, R. Trivedi, "Interdendritic spacing. 1. Experimental studies", *Metall. Trans. A* **15** (1984), p. 967-975.
- [36] P. Kurowski, C. Guthmann, S. Decheveigne, "Shapes, wavelength selection, and the cellular-dendritic transition in directional solidification", *Phys. Rev. A* **42** (1990), p. 7368-7376.
- [37] B. Billia, H. Jamgotchian, H. N. Thi, "Influence of sample thickness on cellular branches and cell-dendrite transition in directional solidification of binary alloys", *J. Cryst. Growth* **167** (1996), p. 265-276.
- [38] S. Liu, M. Suk, L. Fabbietti, R. Trivedi, "The effect of dimensionality on microstructures in directionally solidified SCN-Salol alloys", in *Solidification Processes and Microstructures: A Symposium in Honor of Wilfried Kurz* (M. Rappaz, C. Beckermann, R. Trivedi, eds.), Minerals, Metals & Materials Soc., Pittsburgh, PA, 2004, p. 211-218.
- [39] J. Chen, P. K. Sung, S. N. Tewari, D. R. Poirier, H. C. de Groh, "Directional solidification and convection in small diameter crucibles", *Mater. Sci. Eng.* **357** (2003), p. 397-405.
- [40] J. Chen, S. N. Tewari, G. Magadi, H. C. de Groh, "Effect of crucible diameter reduction on the convection, macrosegregation, and dendritic morphology during directional solidification of Pb-2.2 wt pct Sb alloy", *Metall. Trans. A* **34** (2003), p. 2985-2990.
- [41] J. A. Burton, R. C. Prim, W. P. Slichter, "The distribution of solute in crystals grown from the melt. Part I. Theoretical", *J. Chem. Phys.* **21** (1953), p. 1987-1991.
- [42] J. J. Favier, "Macrosegregation. 2. A comparative-study of theories", *Acta Metall.* **29** (1981), p. 205-214.
- [43] A. Karma, W. J. Rappel, B. C. Fuh, R. Trivedi, "Model of banding in diffusive and convective regimes during directional solidification of peritectic systems", *Metall. Mater. Trans. A* **29** (1998), p. 1457-1470.
- [44] J. A. Warren, J. S. Langer, "Prediction of dendritic spacings in a directional-solidification experiment", *Phys. Rev. E* **47** (1993), p. 2702-2712.
- [45] D. Camel, J. J. Favier, "Thermal-convection and longitudinal macrosegregation in horizontal bridgman crystal-growth. 1. Order of magnitude analysis", *J. Cryst. Growth* **67** (1984), p. 42-56.
- [46] D. Camel, J. J. Favier, "Thermal-convection and longitudinal macrosegregation in horizontal bridgman crystal-growth. 2. Practical laws", *J. Cryst. Growth* **67** (1984), p. 57-67.
- [47] J. J. Favier, "Recent advances in bridgman growth modeling and fluid-flow", *J. Cryst. Growth* **99** (1990), p. 18-29.
- [48] L. Strutzenberg, "Plane front dynamics and pattern formation in diffusion controlled directional solidification of alloys", PhD Thesis, Iowa State University, 2004.
- [49] T. Taenaka, H. Esaka, S. Mizoguchi, H. Kajioaka, "Equilibrium phase diagram of succinonitrile-camphor system", *J. Japan Inst. Metals Mater.* **52** (1988), p. 491-494.
- [50] M. A. Chopra, M. E. Glicksman, N. B. Singh, "Dendritic solidification in binary-alloys", *Metall. Trans. A* **19** (1988), p. 3087-3096.

- [51] F. L. Mota, L. M. Fabietti, N. Bergeon, L. L. Strutzenberg, A. Karma, B. Billia, R. Trivedi, "Quantitative determination of the solidus line in the dilute limit of succinonitrile-camphor alloys", *J. Cryst. Growth* **447** (2016), p. 31-35.
- [52] W. W. Mullins, R. F. Sekerka, "Stability of a planar interface during solidification of a dilute binary alloy", *J. Appl. Phys.* **35** (1964), p. 444-451.
- [53] J. C. LaCombe, J. L. Oudemool, M. B. Koss, L. T. Bushnell, M. E. Glicksman, "Measurement of thermal expansion in liquid succinonitrile and pivalic acid", *J. Cryst. Growth* **173** (1997), p. 167-171.
- [54] M. Schraml, F. Sommer, B. Pur, W. Kohler, G. Zimmermann, V. T. Witusiewicz, L. Sturz, "Measurement of non-isothermal transport coefficients in a near-eutectic succinonitrile/(d)camphor mixture", *J. Chem. Phys.* **150** (2019), article no. 204508.
- [55] Q. Li, C. Beckermann, "Modeling of free dendritic growth of succinonitrile-acetone alloys with thermosolutal melt convection", *J. Cryst. Growth* **236** (2002), p. 482-498.
- [56] J. Teng, S. Liu, "Re-determination of succinonitrile (SCN)-camphor phase diagram", *J. Cryst. Growth* **290** (2006), p. 248-257.
- [57] S. Decheveigne, C. Guthmann, M. M. Lebrun, "Cellular instabilities in directional solidification", *J. Phys.* **47** (1986), p. 2095-2103.
- [58] L. M. Fabietti, V. Seetharaman, R. Trivedi, "The development of solidification microstructures in the presence of lateral constraints", *Metall. Trans. A* **21** (1990), p. 1299-1310.
- [59] J. W. Rutter, B. Chalmers, "A prismatic substructure formed during solidification of metals", *Can. J. Phys.* **31** (1953), p. 15-39.
- [60] W. A. Tiller, K. A. Jackson, J. W. Rutter, B. Chalmers, "The redistribution of solute atoms during the solidification of metals", *Acta Metall.* **1** (1953), p. 428-437.
- [61] D. Camel, J. J. Favier, "Theoretical-analysis of solute transport regimes during crystal-growth from the melt in an ideal czochralski configuration", *J. Cryst. Growth* **61** (1983), p. 125-137.
- [62] J. P. Garandet, T. Alboussiere, "Bridgman growth: modelling and experiments", *Prog. Cryst. Growth Character. Mater.* **38** (1999), p. 73-132.